Published in final edited form as:

Cell Rep. 2014 June 26; 7(6): 1914–1925. doi:10.1016/j.celrep.2014.05.006.

IKKα Promotes Intestinal Tumorigenesis by Limiting Recruitment of M1-like Polarized Myeloid Cells

Serkan I. Göktuna[1,2], **Ozge Canli**[1,3], **Julia Bollrath**[1], **Alexander A. Fingerle**[4], **David Horst**[5], **Michaela A. Diamanti**[1,3], **Charles Pallangyo**[1,3], **Moritz Bennecke**[1], **Tim Nebelsiek**[1], **Arun K. Mankan**[1], **Roland Lang**[6], **David Artis**[7], **Yinling Hu**[8], **Thomas Patzelt**[9], **Jürgen Ruland**[9,10], **Thomas Kirchner**[5,10], **M. Mark Taketo**[11], **Alain Chariot**[2], **Melek C. Arkan**[1], **Florian R. Greten**[1,3,10,*]

[1]Institute of Molecular Immunology, Klinikum rechts der Isar, Technische Universität München, 81675 Munich, Germany

[2]Unit of Signal Transduction (GIGA-ST), GIGA-R, University of Liege and WELBIO, CHU, Sart-Tilman, 4000 Liege, Belgium

[3]Georg-Speyer-Haus, Institute for Tumor Biology and Experimental Therapy, 60596 Frankfurt am Main, Germany

[4]Department of Radiology, Klinikum rechts der Isar, Technische Universität München, 81675 Munich, Germany

[5]Institute of Pathology, Ludwig-Maximilian-University, 80337 Munich, Germany

[6]Institute of Clinical Microbiology, Immunology and Hygiene, University Hospital Erlangen, 91054 Erlangen, Germany

[7]Department of Microbiology and Institute for Immunology, Perelman School of Medicine, University of Pennsylvania, Philadelphia, PA 19104, USA

[8]Laboratory of Experimental Immunology, Cancer and Inflammation Program, Center for Cancer Research, National Cancer Institute at Frederick, Frederick, MD 21701, USA

[9]Department of Clinical Chemistry, Klinikum rechts der Isar, Technische Universität München, 81675 Munich, Germany

[10]German Cancer Consortium (DKTK) and German Cancer Research Center (DKFZ), Im Neuenheimer Feld 280, 69120 Heidelberg, Germany

[11]Department of Pharmacology, Graduate School of Medicine, Kyoto University, Kyoto 606-8501, Japan

SUMMARY

[*]Correspondence: greten@gsh.uni-frankfurt.de.

ACCESSION NUMBERS

Gene expression data have been deposited in the Gene Expression Omnibus database under accession number GSE51631.

SUPPLEMENTAL INFORMATION

Supplemental Information includes two figures and can be found with this article online at http://dx.doi.org/10.1016/j.celrep.2014.05.006.

The recruitment of immune cells into solid tumors is an essential prerequisite of tumor development. Depending on the prevailing polarization profile of these infiltrating leucocytes, tumorigenesis is either promoted or blocked. Here, we identify IκB kinase α (IKKα) as a central regulator of a tumoricidal microenvironment during intestinal carcinogenesis. Mice deficient in IKKα kinase activity are largely protected from intestinal tumor development that is dependent on the enhanced recruitment of interferon γ (IFNγ)-expressing M1-like myeloid cells. In IKKα mutant mice, M1-like polarization is not controlled in a cell-autonomous manner but, rather, depends on the interplay of both IKKα mutant tumor epithelia and immune cells. Because therapies aiming at the tumor microenvironment rather than directly at the mutated cancer cell may circumvent resistance development, we suggest IKKα as a promising target for colorectal cancer (CRC) therapy.

INTRODUCTION

An inflammatory microenvironment is an essential component of epithelial tumors that develop on the basis of chronic inflammatory conditions as well as of those malignancies that emerge in an inflammation-independent manner (Quante et al., 2013). In both instances, recruitment of various types of adaptive and innate immune cells can be observed. Depending on the dominating cell type and polarization profile of the infiltrating cells, tumorigenesis is promoted or suppressed (Grivennikov et al., 2010). Recently, an immune score relying on the intratumoral localization of cytotoxic and memory T cells was established in colorectal cancer (CRC) (Fridman et al., 2012). This immune score has a powerful prognostic value and exemplifies the importance of immune cells for this tumor entity. Moreover, a large number of functional in vivo studies have provided substantial evidence demonstrating a key role of myeloid cells in colorectal cancer as well as other tumor entities (Grivennikov et al., 2010). In analogy to the Th1/Th2 classification of T cells, macrophages have been suggested to be grouped into classically activated M1 (in response to interferon γ [IFNγ] or microbial products) or alternatively activated M2 macrophages (in response to interleukin 4 [IL-4]; Gordon and Taylor, 2005) In the context of tumor-associated macrophages, M1 macrophages are considered to behave in a tumoricidal manner whereas M2 macrophages promote tumorigenesis (Mantovani et al., 2002). However, the exact molecular and cellular basis underlying the tumor-promoting lymphocyte and myeloid cell polarization within the tumor microenvironment is still poorly defined.

Nuclear factor (NF)-κB activation leads to the establishment of a protumorigenic inflammatory microenvironment of various malignancies (Bollrath and Greten, 2009). NF-κB is tightly controlled by the IκB-kinase (IKK) complex, which consists of two catalytic subunits, namely the IKKα and IKKβ proteins, as well as the regulatory subunit IKKγ (Chariot, 2009). The classical NF-κB activation controls key functions for tumor initiation, promotion, and progression both in tumor as well as in infiltrating myeloid cells (Karin and Greten, 2005). In contrast to classical IKKγ/IKKβ-dependent NF-κB signaling, alternative NF-κB activation depends solely on IKKα (Vallabhapurapu and Karin, 2009). Moreover, IKKα comprises a nuclear localization signal and can therefore also confer important nuclear functions (Chariot, 2009). Whereas, in most malignancies, IKKβ-dependent NF-κB signaling clearly promotes tumorigenesis, the role of IKKα in this context is more complex.

Inhibition of IKKα prolongs survival and suppresses occurrence of metastatic diseases in models of mammary and prostate cancer (Cao et al., 2007; Luo et al., 2007; Tan et al., 2011; Zhang et al., 2013). In contrast, loss of IKKα enhances susceptibility to carcinogen-induced squamous cell carcinomas (SCC) in the skin and leads to development of spontaneous lung SCC (Liu et al., 2008; Xiao et al., 2013). Interestingly, the latter depends in part on the development of an excessive inflammatory environment triggered by IKKα mutant macrophages (Xiao et al., 2013).

Globally sporadic CRC comprises the second most common cause of cancer in women and the third most common cause in men (Jemal et al., 2009). In over 80% of the cases, it is initiated by *APC* and *CTNNB* mutations that cause persistent activation of the Wnt pathway (Fearon, 2011). We could recently demonstrate that proinflammatory IKKβ-dependent NF-κB signaling enhances β-catenin promoter binding, causing dedifferentiation of postmitotic epithelia and tumor stem cell expansion during Wnt-dependent tumor initiation (Schwitalla et al., 2013a). Moreover, canonical NF-κB activation controls development of epithelial-mesenchymal transition (EMT) and myeloid cell recruitment in *Tp53*-deficient invasive carcinomas (Schwitalla et al., 2013b). In contrast, IKKα directly phosphorylates β-catenin, thus increasing its abundance to promote cyclin D1 expression (Albanese et al., 2003), and in colorectal cancer cells, an active IKKα isoform was described (Margalef et al., 2012). However, functional genetic evidence supporting a cell autonomous or nonautonomous role of IKKα and/or the alternative NF-κB activation pathway in colorectal carcinogenesis is lacking.

RESULTS

Impaired IKKα Activation Suppresses Intestinal Tumorigenesis

To functionally examine the role of IKKα during early intestinal tumorigenesis, we employed $IKK\alpha^{AA/AA}$ knockin mice, which contain alanines instead of serines in the activation loop of IKKα and express therefore a nonactivatable form of this kinase (Cao et al., 2001). Whereas $IKK\alpha^{AA/AA}$ mice are characterized by impaired development of Peyer's patches (Senftleben et al., 2001), intestinal epithelial cell (IEC) differentiation was indistinguishable from littermate controls. $IKK\alpha^{AA/AA}$ mice displayed regular numbers and distribution of goblet cells, Paneth cells, as well as enteroendocrine cells (data not shown). Similarly, proliferation and apoptosis rates of unchallenged intestinal epithelial cells in small and large intestine were unaltered (data not shown). To induce intestinal tumorigenesis, $IKK\alpha^{AA/AA}$ mice and littermate controls were repetitively challenged with the procarcinogen azoxymethane (AOM), which is commonly used to induce adenoma growth in the distal colon of rodents. Expression of mutant IKKα markedly reduced number of adenomas (>75%) when animals were analyzed 20 weeks after the first carcinogen exposure (Figure 1A). $IKK\alpha^{AA/AA}$ mice developed only few relatively small tumors that displayed slower proliferation rates (Figures 1B and 1C). Instead, in $IKK\alpha^{AA/AA}$ mice multifocal low-grade intraepithelial neoplasia was frequently observed. To confirm the $IKK\alpha^{AA/AA}$-dependent antitumorigenic effect in a genetic model of adenomatous polyposis, we crossed $IKK\alpha^{AA/AA}$ mice to $Apc^{Min/+}$ mice and monitored their survival. Similarly, loss of IKKα function conferred a protective effect and prolonged survival of $Apc^{Min/+}$ mice significantly

(median survival of 236.5 days in homozygous *IKKα*$^{AA/AA}$ mutants versus 184.5 days in heterozygous *IKKα*$^{AA/WT}$ mutants and 166 days in *IKKα*$^{WT/WT}$ wild-type *Apc*$^{Min/+}$ mice; $p < 0.0001$; Figure 1D). Accordingly, when we analyzed 4-month-old *Apc*$^{Min/+}$ animals, tumor incidence and size as well as proliferation of tumor epithelia was significantly decreased in *IKKα*$^{AA/AA}$ mutant mice (Figures 1E–1H; data not shown). Furthermore, consistent with lower tumor burden, anemia—usually developing in *Apc*$^{Min/+}$ mice as tumorigenesis progresses—was normalized in *Apc*$^{Min/+}$/*IKKα*$^{AA/AA}$ compound mutants (Figures 1I and 1J). Collectively, these results suggested that *IKKα*$^{AA/AA}$ mediated antiproliferative effects during early tumor stages, which led to marked tumor suppression in both models of intestinal tumorigenesis.

IKKα$^{AA/AA}$ Mice Block Tumor Cell Proliferation Independently of Alternative NF-κB Activation

Tamoxifen-inducible *β-cat*$^{c.a.}$ mice comprise an excellent model to study Wnt-dependent tumor initiation. These mice are characterized by IEC-restricted stabilization of β-catenin causing rapid expansion of intestinal crypts and loss of differentiated IEC, and within 4 weeks, *β-cat*$^{c.a.}$ mice succumb to this marked crypt hyperproliferation (Schwitalla et al., 2013a). Similarly to the results obtained in AOM-induced and *Apc*-dependent tumor models, mutant IKKα blocked proliferation and expansion of c-myc-expressing β-catenin mutant crypts within 2 weeks after tamoxifen induction (Figures 2A–2C). This was associated with decreased CDK1 and CDK2 activity when mice were analyzed 15 days after the first tamoxifen administration (Figures 2D and 2E). Accordingly, impaired IKKα activation prolonged survival of *β-cat*$^{c.a.}$ mutant animals (Figure 2F). Interestingly, loss of NF-κB2/p100 did not affect survival, indicating that IKKα acted independently of the alternative NF-κB activation pathway (Hayden and Ghosh, 2004). In line with this notion, we also did not observe any differences in p100 processing in *β-cat*$^{c.a.}$/*IKKα*$^{AA/AA}$ IEC (data not shown).

Prolonged Survival of IKKα Mutant *β-cat*$^{c.a.}$ Mice Depends on IFNγ

To further explore the underlying IKKα-controlled proproliferative mechanism, we performed a microarray analysis comparing RNA isolated from wild-type, *IKKα*$^{AA/AA}$, *β-cat*$^{c.a.}$, or *β-cat*$^{c.a.}$/*IKKα*$^{AA/AA}$ IEC 15 days after the first tamoxifen administration. A total of 732 genes were significantly differentially expressed. In IEC from *β-cat*$^{c.a.}$/*IKKα*$^{AA/AA}$ compared to *β-cat*$^{c.a.}$ mice, a general downregulation of Wnt-dependent transcripts rather than control of particular gene subsets was observed. These different transcription profiles supposedly reflected the observed differences in IEC morphology between the two genotypes (Figure 2A), but not distinct IKKα-controlled signaling events. Indeed, knock-down of IKKα did not decrease β-catenin binding to its Tcf/Lef motif in human embryonic kidney 293 cells when transfected with a constitutively active β-catenin mutant (Figure S1). Therefore, we focused our attention on the group of transcripts that were markedly upregulated in IEC from *β-cat*$^{c.a.}$/*IKKα*$^{AA/AA}$ mice. These could be classified into genes associated with immune response and inflammatory functions when sorted by their membership in KEGG pathways (Figure 3A). More specifically, gene set enrichment analysis (GSEA) indicated an enrichment of type I and II IFN targets in *β-cat*$^{c.a.}$/*IKKα*$^{AA/AA}$ IEC (Figure 3B), including *Stat1*, *Irf1*, *Nos2*, *Oas1*, *Pkr*, and *Isg15*, which could be confirmed by real-time PCR (Figure 3C). This was paralleled by a marked

upregulation of IFNγ in whole mucosa of *β-cat*$^{c.a.}$/*IKKα*$^{AA/AA}$ mice (Figure 3D). Moreover, immunoblot analysis confirmed activation of tyrosine-phosphorylated Stat1(Y701) as well as upregulation of Nos2 and IRF-1 in IKKα mutant IEC (Figure 3E). Because IFNγ/Stat1 signaling is known to suppress tumor cell proliferation, this raised the possibility that the decreased IEC proliferation in *β-cat*$^{c.a.}$/*IKKα*$^{AA/AA}$ mice was non-cell-autonomous and IFNγ dependent. To confirm this hypothesis, we either adoptively transferred *IKKα*$^{AA/AA}$ bone marrow to *β-cat*$^{c.a.}$ mice or used conditional *IKKα*$^{F/F}$ mutants to specifically delete IKKα in *β-cat*$^{c.a.}$ IEC (Liu et al., 2008). IEC-restricted deletion of IKKα only moderately protected *β-cat*$^{c.a.}$ mice (Figure 4A). In contrast, adoptive transfer of *IKKα*$^{AA/AA}$ bone marrow extended survival of *β-cat*$^{c.a.}$ mice almost to the same extent as it was otherwise seen in *IKKα*$^{AA/AA}$ whole-body mutants (Figure 4B). More importantly, loss of *Ifng*, but not blocking type I interferon signaling by *Ifnar* deletion, completely prevented IKKα-mediated survival advantage (Figure 4C). Collectively, these data provided clear evidence that mutant IKKα suppressed IEC proliferation in a paracrine type II interferon-dependent manner.

IKKα$^{AA/AA}$ Myeloid Cells Rather Than T or NK Cells Comprise the Source of IFNγ

The most common IFNγ-expressing cell types in the lamina propria are T and natural killer (NK) cells. Surprisingly, we did not detect any difference in the number of mucosa-infiltrating CD3$^+$ T cells by immunohistochemistry (Figure 5A). Moreover, fluorescence-activated cell sorting (FACS) analysis did not indicate changes in the number of CD4$^+$IFNγ$^+$ or CD8$^+$IFNγ$^+$ T cells between *β-cat*$^{c.a.}$ and *β-cat*$^{c.a.}$/*IKKα*$^{AA/AA}$ mice when animals were analyzed 15 days after the first tamoxifen administration (Figure 5B). Moreover, when we differentiated naive T cells from either wild-type or *Ikkα*$^{AA/AA}$ animals into either Th_1 or Th_2 cells ex vivo, we were not able to determine any significant changes between the two genotypes (Figure S2A). Consequently, athymic nude mice (NU-*Foxn1*^{nu}) that lack T cells did not revert the survival advantage of *β-cat*$^{c.a.}$/*Ikkα*$^{AA/AA}$ mice (data not shown). In addition, also depletion of NK cells using α-asialo-GM-1 antibody (reduction of >90% of splenic DX5$^+$ cells was confirmed by FACS; data not shown) did not affect survival of *β-cat*$^{c.a.}$/*Ikkα*$^{AA/AA}$ mice (Figure 5C), indicating that neither CD4$^+$, CD8$^+$ T cells, nor NK cells were responsible for the IFNγ-mediated survival extension of *Ikkα*$^{AA/AA}$ mutant *β-cat*$^{c.a.}$ mice.

During carcinogenesis, polarization of myeloid cells into M1 or M2 macrophages or in the case of neutrophils into N1 or N2 has been suggested to play an important role for tumor development (Sica and Mantovani, 2012). Depending on the prevailing polarization profile, M1 macrophages (typically expressing *Ifng, Tnfa, Il12, Nos2, Cxcl9, Cxcl10*, and *Cxcl11*) are considered tumoricidal, whereas M2 macrophages (characterized by high levels of *Arg1, Mrc1, Ccl17, Ccl22, Ym1*, and *Fizz1*) have been suggested to promote tumorigenesis (Sica and Mantovani, 2012). Considering the lack of T and NK cell involvement in the pronounced expression of *Nos2* and *Ifng*, we speculated that instead a general shift in macrophage polarization toward M1 could have been responsible for this. Indeed, besides *Nos2* and *Ifng*, expression of several other genes encoding M1 markers were elevated in the lamina propria of *β-cat*$^{c.a.}$/*Ikkα*$^{AA/AA}$ mice 15 days after the first tamoxifen administration, whereas only *Ccl17* among M2-associated genes was downregulated (Figure 6A). To

examine whether *IKKα*$^{AA/AA}$ mutant macrophages per se would reveal an M1 phenotype, we stimulated bone-marrow-derived macrophages (BMDM) under M1- or M2-polarizing conditions. Interestingly, ex vivo *Ikkα*$^{AA/AA}$ macrophages did not reveal an enhanced M1 polarization profile compared to control BMDM and did not show a preferred polarization (Figure 6B). Moreover, also *Ifng* expression was indifferent when BMDM of either genotype were stimulated with a combination of IL-12 and IL-18 (Figure S2C), thus ruling out a cell autonomous regulation in the generation of *Ikkα*$^{AA/AA}$ M1-like cells in vivo.

Elevated expression levels of myeloid-recruiting chemokines such as *Cxcl1, Cxcl2, Cxcl5*, and *Ccl2* (Figure 6C) led to enhanced recruitment of macrophages, neutrophils, and dendritic cells into the lamina propria of *β-cat*$^{c.a.}$/*Ikkα*$^{AA/AA}$ mutants, as determined by real-time PCR of genes encoding surface markers *Emr1, Ly6g*, and *Itgax* (Figure 6D) as well as by FACS analysis (data not shown). Only *Cxcl1* and *Cxcl2* upregulation was observed in IKKα mutant epithelia (Figure 6C), indicating that *Cxcl5* and *Ccl2* were derived from infiltrating immune cells. Interestingly, apart from enhanced myeloid cell recruitment, also localization of both macrophages and neutrophils was distinct in *β-cat*$^{c.a.}$/*Ikkα*$^{AA/AA}$ mice, where they could be found interspersed in between IEC. In contrast, infiltration of F4/80^{+} and Gr-1^{+} myeloid cells was limited to the villus stroma in IKKα wild-type-expressing *β-cat*$^{c.a.}$ mice (Figures 6E–6H). Importantly, immunofluorescence confirmed that indeed both macrophages and neutrophils expressed IFNγ (Figures 6I and 6J), indicating that an enhanced recruitment of M1-like myeloid cells was responsible for the IFNγ-dependent survival advantage of *β-cat*$^{c.a.}$/*Ikkα*$^{AA/AA}$ mice.

Enhanced Recruitment of Myeloid Cells Depends on IKKβ Activation in *β-cat*$^{c.a.}$/*Ikkα*$^{AA/AA}$ IEC

Myeloid-cell-recruiting chemokines such as Cxcl1, Cxcl2, Cxcl5, and Ccl2 are controlled by classical NF-κB activation (Grivennikov et al., 2010). To functionally confirm that indeed the enhanced recruitment of M1-like myeloid cells was responsible for the extended survival in *β-cat*$^{c.a.}$/*Ikkα*$^{AA/AA}$ mice, we reasoned that loss of IKKβ-dependent NF-κB activation in IEC should block recruitment of myeloid cells in IKKα mutant *β-cat*$^{c.a.}$ animals. Thus, we intercrossed floxed *Ikk*β mutants (*Ikk*β$^{F/F}$) with *β-cat*$^{c.a.}$/*Ikkα*$^{AA/AA}$ mice to generate *β-cat*$^{c.a.}$/*Ikkα*$^{AA/AA}$/*Ikkβ*$^{\Delta IEC}$ as well as *β-cat*$^{c.a.}$/*Ikkβ*$^{\Delta IEC}$ compound mutants. Expectedly, IKKβ deletion decreased *Cxcl1* and *Ccl2* as well as *Emr1, Ly6g*, and *Itgax* expression and prevented *Ifng* upregulation (Figure 7A). Immunofluorescence confirmed diminished F4/80^{+} and Gr-1^{+} cell infiltration into mucosa of *β-cat*$^{c.a.}$/*Ikkα*$^{AA/AA}$/*Ikkβ*$^{\Delta IEC}$ animals (Figures 7B–7E). We recently demonstrated that loss of RelA/p65 expanded the life span of *β-cat*$^{c.a.}$ mice (Schwitalla et al., 2013a). Similarly, deletion of *Ikk*β prolonged survival of *Ctnnb* mutants (Figure 7F). However, consistent with a lack of *Ifng* induction, *β-cat*$^{c.a.}$/*Ikkα*$^{AA/AA}$ animals were no longer protected in the absence of IKKβ and their survival was now comparable to that of *β-cat*$^{c.a.}$/*Ikkβ*$^{\Delta IEC}$ mice (Figure 7F). Thus, these data further supported the importance of IFNγ-expressing myeloid cells for the survival of *β-cat*$^{c.a.}$/*Ikkα*$^{AA/AA}$ mice and confirmed that M1-like polarization did not occur in a cell autonomous manner in IKKα mutant myeloid cells.

DISCUSSION

Cell plasticity is an important phenomenon during carcinogenesis that affects basically all cells in the tumor microenvironment (Hanahan and Weinberg, 2011). Whereas induction of EMT altering tumor cells themselves is an essential prerequisite for invasion and metastasis, polarization of infiltrating immune cells provides the microenvironment-dominating cytokine milieu, which ultimately controls behavior of resident stromal and tumor cells. Depending on the cytokine milieu, carcinogenesis is promoted or suppressed (Grivennikov et al., 2010). To decipher the cellular and molecular mechanisms that shape the cytokine milieu bears great therapeutic potential, because cytokine-producing immune cells are unlikely to develop resistance mechanisms in contrast to mutagenized tumor cells. Although IKKα has been suggested to control various cell autonomous tumor-promoting mechanisms in CRC (Albanese et al., 2003; Margalef et al., 2012), here we provide evidence that IKKα comprises a central regulatory element in the suppression of M1-like myeloid cell controlled microenvironment rather than directly stimulating tumor cell proliferation. Elevated IFNγ levels in $Ikk\alpha^{AA/AA}$ mucosa are most likely responsible for growth arrest of initiated epithelial cells. However, considering the particular intraepithelial localization of myeloid cells in $\beta\text{-}cat^{c.a.}/Ikk\alpha^{AA/AA}$ mice, we cannot rule out the possibility that these cells may also participate either in extracellular killing or phagocytosis of tumor cells as it was recently demonstrated using oncogenic HRAS(G12V)-transformed cells in zebrafish larvae (Feng et al., 2010).

Importantly, polarization of IKKα mutant myeloid cells depends on a complex interplay of IEC and infiltrating cells and is not a cell autonomously controlled process. Instead, it involves classical NF-κB-dependent secretion of chemokines in $Ikk\alpha^{AA/AA}$ IEC that triggers recruitment of myeloid cells, which in turn secrete cytokines that culminate in M1 polarization and fuel into a feedforward loop that drives IFNγ secretion. This is further supported by the fact that administration of IL-12-neutralizing antibodies is not sufficient to block this loop and to prevent IFNγ secretion (S.I.G. and F.R.G., unpublished data). However, prevention of myeloid cell infiltration and subsequent ablation of M1-like polarization can be achieved by inhibition of NF-κB activation in IEC. Considering that IKKα expression correlates with poor prognosis in human Union for International Cancer Control stage II CRC (S.I.G. and F.R.G., unpublished data), whereas IFNγ upregulation is associated with improved survival (Grenz et al., 2013), IKKα may represent a valuable therapeutic target for CRC therapy or prevention. If, however, putative IKKα inhibitors were indeed at some point considered for CRC therapy, our data imply that such compounds are required to be highly specific inhibitors of only IKKα because simultaneous overlapping IKKβ inhibition would most likely prevent the beneficial effects of selective IKKα inhibition.

We recently demonstrated that, during Wnt-initiated tumorigenesis, NF-κB activation cooperates with β-catenin to control dedifferentiation of postmitotic epithelia and stem cell expansion (Schwitalla et al., 2013a). Although in IKKα mutant IEC chemokine expression is enhanced in an NF-κB-dependent manner, we do not have any evidence that Wnt signaling is enhanced in $Ikk\alpha^{AA/AA}$ IEC as well. This supports the notion that IKKα is

responsible for the negative regulation of a very distinct set of NF-κB target genes only (Lawrence et al., 2005; Schwitalla et al., 2013a).

Depending on the type of malignancy, IKKα can provide both tumor-promoting and tumor-suppressive mechanisms that are in most instances cell autonomous. IKKα controls expression of the inhibitor of metastasis maspin in breast and prostate cancer (Luo et al., 2007; Tan et al., 2011) and is required for ErbB2-induced mammary tumorigenesis. In the latter case, NIK-dependent IKKα activation regulates expansion of tumor-initiating cells by directly phosphorylating the cyclin-dependent kinase inhibitor p27 (Zhang et al., 2013). Additional tumor-promoting nuclear functions of IKKα include cell cycle regulation and chromosomal accessibility by phosphorylation of histone H3, AuroraB kinase, or the nuclear corepressor SMRT, which triggers its nuclear export with HDAC3 and its degradation (Chariot, 2009). In contrast, IKKα acts as a tumor suppressor in models of skin or lung SCC (Liu et al., 2008; Xiao et al., 2013). Importantly, during development of lung SCC, IKKα kinase inactivation culminates in the recruitment of tumor-promoting inflammatory macrophages and depletion of macrophages prevents SCC formation (Xiao et al., 2013). This is in clear contrast to our findings presented here, yet the reason for this diverse macrophage activation profile in these two different tumor entities remains currently unclear. One could envision that specific alterations in the intestinal microbiome of *Ikkα*$^{AA/AA}$ mice may be involved in the tumor-suppressive M1 polarization of myeloid cells that only becomes apparent after barrier defect causing oncogene activation (Grivennikov et al., 2012).

EXPERIMENTAL PROCEDURES

Mice

IKKα$^{AA/AA}$ (Cao et al., 2001), *IKKα*$^{F/F}$ (Liu et al., 2008), *Ikkβ*$^{F/F}$ (Greten et al., 2004), *Nfkb2*$^{-/-}$ (Paxian et al., 2002), and *β-cat*$^{c.a.}$ (Schwitalla et al., 2013a) mice have been recently described. C57BL/6Apc$^{Min/+}$, *Ifng*$^{-/-}$, and *NU-Foxn1*^{nu} mice were purchased from the Jackson Laboratories, and *Ifnar*$^{-/-}$ mice were provided by F. Schmitz, TU Munich. To examine AOM-induced tumorigenesis, mice had been backcrossed to a FVB background for four generations, and littermate controls were used in all experiments. Before crossing to C57BL/6*Apc*$^{Min/+}$ mice, *IKKα*$^{AA/AA}$ animals had been backcrossed to a C57BL/6 background for eight generations. Experiments using *β-cat*$^{c.a.}$ mutants were performed on a mixed C57BL/6 × 129Sv × FVB background, and in all experiments, littermate controls were used. Tamoxifen (Sigma; 1 mg in an ethanol/sunflower oil mixture) was applied by oral gavage on 5 consecutive days. Azoxymethane (10 mg/kg; Sigma) was injected intraperitoneally (i.p.) once weekly for 6 weeks. In adoptive transfer experiments, recipient mice were irradiated (9 Gy) and 2 × 10^6 bone marrow cells from *IKKα*$^{AA/AA}$ mice or *IKKα*$^{WT/WT}$ littermate controls were transferred by tail vein injection. Eight weeks after transplantation, tamoxifen administration was started. To deplete NK cells, 200 μg α-Asialo GM1 antibody (no. 986–10001; Wako) was injected i.p. every 4 days. All procedures were reviewed and approved by the Regierung von Oberbayern.

Protein Analysis

Isolation of enterocytes, immunoblot analysis, immune complex kinase assay, and DNA affinity precipitation assay were performed as described previously (Bollrath et al., 2009; Schwitalla et al., 2013a). The following antibodies were used: anti-IKKα (IMG136A; Imgenex), anti-IKKβ (05–535; Upstate), anti-β-actin (A4700; Sigma), anti-β-catenin (UBI 6734; United Bio Research), anti-phospho-STAT1 (9171; Cell Signaling Technology), anti-STAT1 (SC-346; Santa Cruz Biotechnology), anti-c-Myc (SC-788), anti-IRF-1 (SC-640), anti-NOS2 (SC-651), anti-Cdc2 (SC-54), anti-Cdk2 (SC-163), anti-Cdk4 (SC-260), and anti-β-catenin (SC-1496).

Histological Procedures and Flow Cytometry

Standard immunohistochemical procedures were performed using the following antibodies: anti-bromodeoxyuridine (BrdU) antibody (RPN201; GE Healthcare), anti-IKKα (Abcam; ab109749; clone EPR464), CD68 (Fisher Scientific; MS-397; clone KP1), anti-c-*myc* (SC-788), anti-F4/80 (Caltag; MF 480043), anti-Gr-1 (eBioscience; 12–5931-85), and anti-IFNγ (R&D Systems; BAF 485). For the isolation of lamina propria cells, intestines of mice were opened longitudinally, cleared of mucus, chopped into small pieces, and shook in Hank's balanced salt solution (Invitrogen) containing 30 mM EDTA (Sigma-Aldrich) at 37°C for 20 min followed by 30 s of heavy vortexing to detach the epithelial layer. The remaining tissue pieces were washed at least five times in PBS and then digested in RPMI (Invitrogen) containing 1 mg/ml collagenase I (Sigma-Aldrich) and 20 μg/ml DNase I (Sigma-Aldrich) for 90 min at 37°C while gently shaking. Liberated cells were then washed in RPMI containing 10% fetal calf serum (Biochrom) and 1% penicillin-streptomycin (Invitrogen). T cells were restimulated using phorbol myristate acetate (PMA) (20 ng/ml) and ionomycin (1 μg/ml) for 6 hr in the presence of Brefeldin A (10 μg/ml; Sigma-Aldrich). Flow cytometric analysis was performed on a Gallios flow cytometer (Beckman Coulter Genomics) or a FACSCalibur (Becton Dickinson), and results were analyzed using FlowJo software (Tree Star). The following fluorochrome-conjugated antibodies were used: fluorescein isothiocyanate-anti-CD4 (BD-557653), phycoerythrin (PE)-anti-CD4 (BD-553651), PE-anti-CD8 (BD-550798), and PE-anti-IFNγ (BD-554412).

RNA Analysis

Total RNA extraction, cDNA synthesis, real-time PCR and gene expression profiling, and GSEA were performed as described previously (Bennecke et al., 2010). Primer sequences are available on request. In GSEA, we matched various interferon-related gene sets from GSEA Software Database (Bosco et al., 2010; Browne et al., 2001; Einav et al., 2005; Natsume et al., 2005; Zhang et al., 2005), Reactome database (http://www.reactome.org/cgi-bin/eventbrowser_st_id?ST_ID=REACT_25229), and STKE database to all transcripts from the Affymetrix Mouse Genome 430A 2.0 Array, respectively. GSEA software is available from Broad Institute of MIT and Harvard University (http://www.broadinstitute.org/gsea/index.jsp). We acknowledge the use of GSEA software (Subramanian et al., 2005) to validate correlation between molecular pathways signatures in any phenotype of interest. For the analysis of gene sets, we modified default parameters as follows: permutation number to

1,000, collapse data set to gene symbols if “false,” permutation type to gene sets, and only gene sets with the size of 1–2,000 signatures were used for analysis.

In Vitro Antigen Presentation Assay

Bone-marrow-derived dendritic cells (BMDC) were differentiated from wild-type (WT) and *IKKα*$^{AA/AA}$ bone marrow in RPMI supplemented with 20 ng/ml GM-CSF for 7 days. On day 7, BMDCs were loaded with ovalbumin (0.5 mg/ml) at 37°C for 1 hr. T cells from spleens of OT II mice (Jackson Laboratories) were purified using a CD4$^+$CD62L$^+$ T cell isolation Kit (Miltenyi Biotech) and carboxyfluorescein succinimidyl ester (CFSE)-labeled (5 μM; 10 min; 37°C). In 96-well plates, 1×10^4 BMDCs were coincubated with 1×10^5 CFSE-labeled OT II cells for 72 hr. Subsequently, cultures were stimulated with PMA (20 ng/ml) for 6 hr, T cell proliferation was analyzed by FACS analysis on a FACS Calibur, and IFNγ production was determined by ELISA.

Directed Differentiation of Naive CD4$^+$ T Cells

Purified naive T_H cells (CD4$^+$CD62L$^+$) were stimulated with anti-CD28 antibody (2 mg/ml; eBioscience) and anti-CD3e-antibody (145–2C11; 5 μg/ml; eBioscience), which had been bound to cell culture plates by anti-Syrian hamster antibody (10 μg/ml; Jackson ImmunoResearch). Cells were directed into the T_H1 line by treatment with IL-12 (2 ng/ml; R&D Systems). Anti-IL-4 antibody was added (10 μg/ml; BD Biosciences) to prevent differentiation toward the T_H2 line. Differentiation toward the T_H2 line was achieved using IL-4 (10 ng/ml; R&D Systems) in the presence of anti-IFN-γ antibody (10 μg/ml; eBioscience) to suppress differentiation into T_H1 cells. Cells were collected for real-time PCR analysis, and RNA was isolated using TRI reagent (Sigma-Aldrich). To confirm successful differentiation, cells were tested for their capacity to produce IFN-γ (T_H1) or IL-4 (T_H2). For that purpose, cells were harvested after the 3-day stimulation, washed, and incubated without stimulus but in presence of IL-2 (10 ng/ml; R&D Systems) for 3 additional days. Afterward, the cells were collected, restimulated with plate-bound anti-CD3 antibody (see above) in the presence of Brefeldin A (10 μg/ml, Sigma-Aldrich), and intracellular cytokine staining was performed.

Statistical Analysis

Data are expressed as mean ± SE. Statistical analysis methods were standard two-tailed Student’s t test for two data sets and ANOVA followed by Bonferroni post hoc test for multiple data sets or log rank test for Kaplan-Meier survival graphs using Prism4 (GraphPad Software) or SPSS Statistics 21. p values ≤ 0.05 were considered significant.

Supplementary Material

Refer to Web version on PubMed Central for supplementary material.

ACKNOWLEDGMENTS

We thank Kerstin Burmeister, Saskia Ettl, Kristin Retzlaff, Birgit Wittig, and Andrea Sendlhofert for technical assistance. We are grateful to Michael Karin for generously providing *IKKα*$^{AA/AA}$ and *Ikkβ*$^{F/F}$ mice as well as Frank Schmitz and Roland M. Schmid for providing *Ifnar*$^{-/-}$ and *Nfkb2*$^{-/-}$ mice, respectively. We thank Jörg

Mages for performing microarray experiments. This work was supported by grants from the Deutsche Krebshilfe (108872), Deutsche Forschungsgemeinschaft (GR 1916/3–1), and the European Research Council (ERC 281967) to F.R.G. Further support was provided by the LOEWE Center for Cell and Gene Therapy Frankfurt (funded by the Hessian Ministry of Higher Education, Research and the Arts; III L 4- 518/17.004).

REFERENCES

Albanese C, Wu K, D'Amico M, Jarrett C, Joyce D, Hughes J, Hulit J, Sakamaki T, Fu M, Ben-Ze'ev A, et al. (2003). IKKalpha regulates mitogenic signaling through transcriptional induction of cyclin D1 via Tcf. Mol. Biol. Cell 14, 585–599. [PubMed: 12589056]

Bennecke M, Kriegl L, Bajbouj M, Retzlaff K, Robine S, Jung A, Arkan MC, Kirchner T, and Greten FR (2010). Ink4a/Arf and oncogene-induced senescence prevent tumor progression during alternative colorectal tumorigenesis. Cancer Cell 18, 135–146. [PubMed: 20708155]

Bollrath J, and Greten FR (2009). IKK/NF-kappaB and STAT3 pathways: central signalling hubs in inflammation-mediated tumour promotion and metastasis. EMBO Rep. 10, 1314–1319. [PubMed: 19893576]

Bollrath J, Phesse TJ, von Burstin VA, Putoczki T, Bennecke M, Bateman T, Nebelsiek T, Lundgren-May T, Canli O, Schwitalla S, et al. (2009). gp130-mediated Stat3 activation in enterocytes regulates cell survival and cell-cycle progression during colitis-associated tumorigenesis. Cancer Cell 15, 91–102. [PubMed: 19185844]

Bosco A, Ehteshami S, Stern DA, and Martinez FD (2010). Decreased activation of inflammatory networks during acute asthma exacerbations is associated with chronic airflow obstruction. Mucosal Immunol. 3, 399–409. [PubMed: 20336062]

Browne EP, Wing B, Coleman D, and Shenk T (2001). Altered cellular mRNA levels in human cytomegalovirus-infected fibroblasts: viral block to the accumulation of antiviral mRNAs. J. Virol. 75, 12319–12330. [PubMed: 11711622]

Cao Y, Bonizzi G, Seagroves TN, Greten FR, Johnson R, Schmidt EV, and Karin M (2001). IKKαalpha provides an essential link between RANK signaling and cyclin D1 expression during mammary gland development. Cell 107, 763–775. [PubMed: 11747812]

Cao Y, Luo JL, and Karin M (2007). IkappaB kinase alpha kinase activity is required for self-renewal of ErbB2/Her2-transformed mammary tumor-initiating cells. Proc. Natl. Acad. Sci. USA 104, 15852–15857. [PubMed: 17890319]

Chariot A (2009). The NF-kappaB-independent functions of IKK subunits in immunity and cancer. Trends Cell Biol. 19, 404–413. [PubMed: 19648011]

Einav U, Tabach Y, Getz G, Yitzhaky A, Ozbek U, Amariglio N, Izraeli S, Rechavi G, and Domany E (2005). Gene expression analysis reveals a strong signature of an interferon-induced pathway in childhood lymphoblastic leukemia as well as in breast and ovarian cancer. Oncogene 24, 6367–6375. [PubMed: 16007187]

Fearon ER (2011). Molecular genetics of colorectal cancer. Annu. Rev. Pathol 6, 479–507. [PubMed: 21090969]

Feng Y, Santoriello C, Mione M, Hurlstone A, and Martin P (2010). Live imaging of innate immune cell sensing of transformed cells in zebrafish larvae: parallels between tumor initiation and wound inflammation. PLoS Biol. 8, e1000562. [PubMed: 21179501]

Fridman WH, Pagès F, Sautè s-Fridman C, and Galon J (2012). The immune contexture in human tumours: impact on clinical outcome. Nat. Rev. Cancer 12, 298–306. [PubMed: 22419253]

Gordon S, and Taylor PR (2005). Monocyte and macrophage heterogeneity. Nat. Rev. Immunol 5, 953–964. [PubMed: 16322748]

Grenz S, Naschberger E, Merkel S, Britzen-Laurent N, Schaal U, Konrad A, Aigner M, Rau TT, Hartmann A, Croner RS, et al. (2013). IFN-γ-driven intratumoral microenvironment exhibits superior prognostic effect compared with an IFN-α-driven microenvironment in patients with colon carcinoma. Am. J. Pathol 183, 1897–1909. [PubMed: 24121019]

Greten FR, Eckmann L, Greten TF, Park JM, Li ZW, Egan LJ, Kagnoff MF, and Karin M (2004). IKKbeta links inflammation and tumorigenesis in a mouse model of colitis-associated cancer. Cell 118, 285–296. [PubMed: 15294155]

Grivennikov SI, Greten FR, and Karin M (2010). Immunity, inflammation, and cancer. Cell 140, 883–899. [PubMed: 20303878]

Grivennikov SI, Wang K, Mucida D, Stewart CA, Schnabl B, Jauch D, Taniguchi K, Yu GY, Osterreicher CH, Hung KE, et al. (2012). Adenomalinked barrier defects and microbial products drive IL-23/IL-17-mediated tumour growth. Nature 491, 254–258. [PubMed: 23034650]

Hanahan D, and Weinberg RA (2011). Hallmarks of cancer: the next generation. Cell 144, 646–674. [PubMed: 21376230]

Hayden MS, and Ghosh S (2004). Signaling to NF-kappaB. Genes Dev. 18, 2195–2224. [PubMed: 15371334]

Jemal A, Siegel R, Ward E, Hao Y, Xu J, and Thun MJ (2009). Cancer statistics, 2009. CA Cancer J. Clin 59, 225–249. [PubMed: 19474385]

Karin M, and Greten FR (2005). NF-kappaB: linking inflammation and immunity to cancer development and progression. Nat. Rev. Immunol 5, 749–759. [PubMed: 16175180]

Lawrence T, Bebien M, Liu GY, Nizet V, and Karin M (2005). IKKalpha limits macrophage NF-kappaB activation and contributes to the resolution of inflammation. Nature 434, 1138–1143. [PubMed: 15858576]

Liu B, Xia X, Zhu F, Park E, Carbajal S, Kiguchi K, DiGiovanni J, Fischer SM, and Hu Y (2008). IKKalpha is required to maintain skin homeostasis and prevent skin cancer. Cancer Cell 14, 212–225. [PubMed: 18772111]

Luo JL, Tan W, Ricono JM, Korchynskyi O, Zhang M, Gonias SL, Cheresh DA, and Karin M (2007). Nuclear cytokine-activated IKKαlpha controls prostate cancer metastasis by repressing Maspin. Nature 446, 690–694. [PubMed: 17377533]

Mantovani A, Sozzani S, Locati M, Allavena P, and Sica A (2002). Macrophage polarization: tumor-associated macrophages as a paradigm for polarized M2 mononuclear phagocytes. Trends Immunol 23, 549–555. [PubMed: 12401408]

Margalef P, Fernández-Majada V, Villanueva A, Garcia-Carbonell R, Iglesias M, López L, Martínez-Iniesta M, Villà-Freixa J, Mulero MC, Andreu M, et al. (2012). A truncated form of IKKα is responsible for specific nuclear IKK activity in colorectal cancer. Cell Reports 2, 840–854. [PubMed: 23041317]

Natsume A, Ishii D, Wakabayashi T, Tsuno T, Hatano H, Mizuno M, and Yoshida J (2005). IFN-beta down-regulates the expression of DNA repair gene MGMT and sensitizes resistant glioma cells to temozolomide. Cancer Res. 65, 7573–7579. [PubMed: 16140920]

Paxian S, Merkle H, Riemann M, Wilda M, Adler G, Hameister H, Liptay S, Pfeffer K, and Schmid RM (2002). Abnormal organogenesis of Peyer's patches in mice deficient for NF-kappaB1, NF-kappaB2, and Bcl-3. Gastroenterology 122, 1853–1868. [PubMed: 12055593]

Quante M, Varga J, Wang TC, and Greten FR (2013). The gastrointestinal tumor microenvironment. Gastroenterology 145, 63–78. [PubMed: 23583733]

Schwitalla S, Fingerle AA, Cammareri P, Nebelsiek T, Göktuna SI, Ziegler PK, Canli O, Heijmans J, Huels DJ, Moreaux G, et al. (2013a). Intestinal tumorigenesis initiated by dedifferentiation and acquisition of stem-cell-like properties. Cell 152, 25–38. [PubMed: 23273993]

Schwitalla S, Ziegler PK, Horst D, Becker V, Kerle I, Begus-Nahrmann Y, Lechel A, Rudolph KL, Langer R, Slotta-Huspenina J, et al. (2013b). Loss of p53 in enterocytes generates an inflammatory microenvironment enabling invasion and lymph node metastasis of carcinogen-induced colorectal tumors. Cancer Cell 23, 93–106. [PubMed: 23273920]

Senftleben U, Cao Y, Xiao G, Greten FR, Krähn G, Bonizzi G, Chen Y, Hu Y, Fong A, Sun SC, and Karin M (2001). Activation by IKKalpha of a second, evolutionary conserved, NF-kappa B signaling pathway. Science 293, 1495–1499. [PubMed: 11520989]

Sica A, and Mantovani A (2012). Macrophage plasticity and polarization: in vivo veritas. J. Clin. Invest 122, 787–795. [PubMed: 22378047]

Subramanian A, Tamayo P, Mootha VK, Mukherjee S, Ebert BL, Gillette MA, Paulovich A, Pomeroy SL, Golub TR, Lander ES, and Mesirov JP (2005). Gene set enrichment analysis: a knowledge-based approach for interpreting genome-wide expression profiles. Proc. Natl. Acad. Sci. USA 102, 15545–15550. [PubMed: 16199517]

Tan W, Zhang W, Strasner A, Grivennikov S, Cheng JQ, Hoffman RM, and Karin M (2011). Tumour-infiltrating regulatory T cells stimulate mammary cancer metastasis through RANKL-RANK signalling. Nature 470, 548–553. [PubMed: 21326202]

Vallabhapurapu S, and Karin M (2009). Regulation and function of NF-kappaB transcription factors in the immune system. Annu. Rev. Immunol 27, 693–733. [PubMed: 19302050]

Xiao Z, Jiang Q, Willette-Brown J, Xi S, Zhu F, Burkett S, Back T, Song NY, Datla M, Sun Z, et al. (2013). The pivotal role of IKKα in the development of spontaneous lung squamous cell carcinomas. Cancer Cell 23, 527–540. [PubMed: 23597566]

Zhang W, Yang H, Kong X, Mohapatra S, San Juan-Vergara H, Hellermann G, Behera S, Singam R, Lockey RF, and Mohapatra SS (2005). Inhibition of respiratory syncytial virus infection with intranasal siRNA nanoparticles targeting the viral NS1 gene. Nat. Med 11, 56–62. [PubMed: 15619625]

Zhang W, Tan W, Wu X, Poustovoitov M, Strasner A, Li W, Borcherding N, Ghassemian M, and Karin M (2013). A NIK-IKKα module expands ErbB2-induced tumor-initiating cells by stimulating nuclear export of p27/Kip1. Cancer Cell 23, 647–659. [PubMed: 23602409]

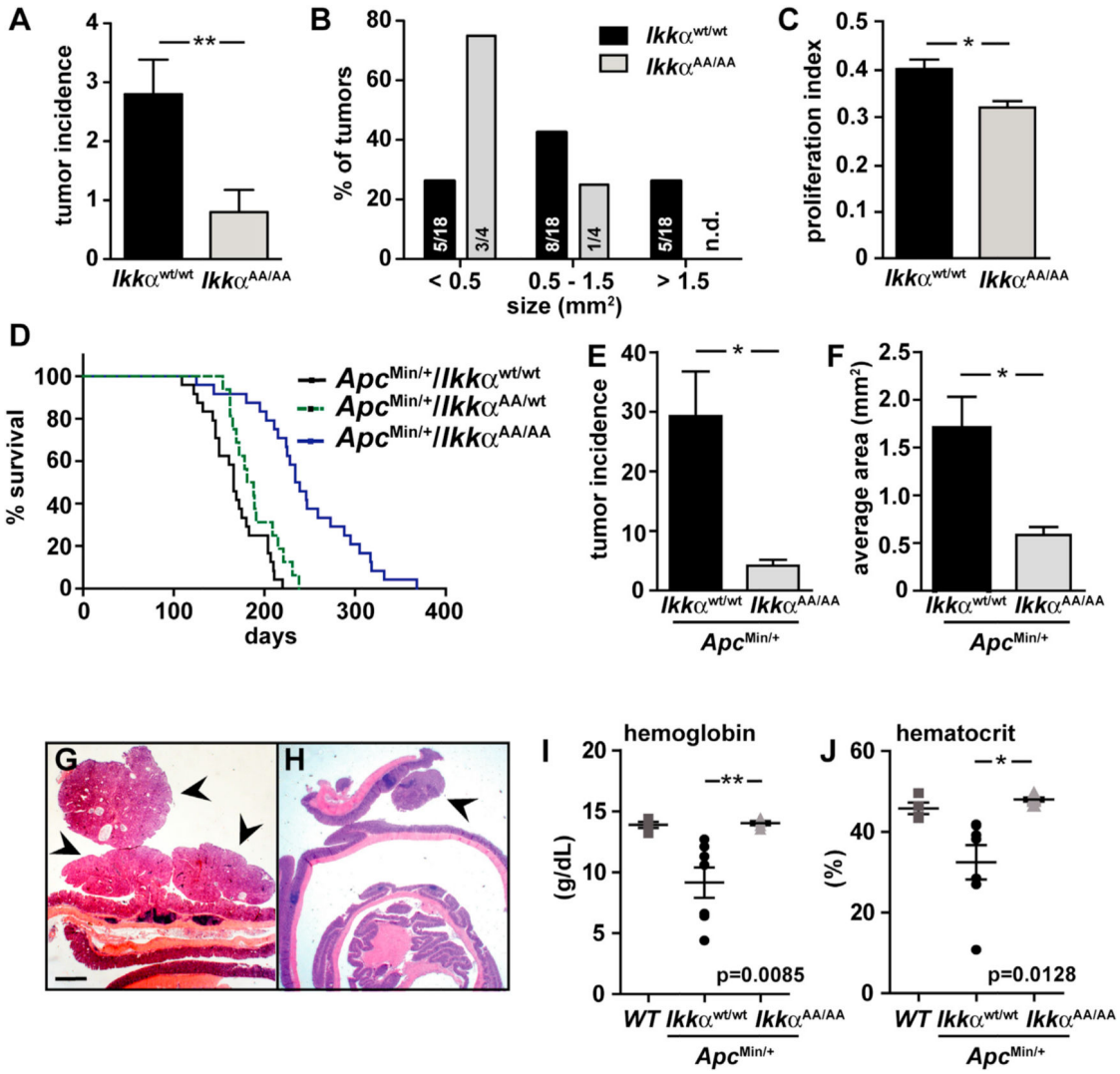

Figure 1. Block of IKKα Activation Impairs Development of Carcinogen and Genetically Induced Intestinal Tumor Models

(A) Tumor incidence of *IKKα*$^{WT/WT}$ and *IKKα*$^{AA/AA}$ mice 20 weeks after the first of six weekly AOM treatments. Data are mean ± SE; n = 5 mice of each genotype; **p < 0.01 by t test.

(B) Size distribution of AOM-induced tumors in *IKKα*$^{WT/WT}$ (n = 18) and *IKKα*$^{AA/AA}$ (n = 4) mice; n.d., not detectable; tumors of this size were not observed in *IKKα*$^{AA/AA}$ mice.

(C) BrdU proliferation index of *IKKα*$^{WT/WT}$ and *IKKα*$^{AA/AA}$ tumor epithelia. Data are mean ± SE; n ≥ 3 tumors of each genotype; *p < 0.05 by t test.

(D) Kaplan-Meier survival curve of *Apc*$^{Min/+}$/*IKKα*$^{WT/WT}$ (n = 24), *Apc*$^{Min/+}$/*IKKα*$^{WT/AA}$ (n = 16), and *Apc*$^{Min/+}$/*IKKα*$^{AA/AA}$ (n = 24); ***p < 0.0001 by log rank test.

(E) Tumor incidence in small intestine and colon of *Apc*$^{Min/+}$/*IKKα*$^{WT/WT}$ and *Apc*$^{Min/+}$/*IKKα*$^{AA/AA}$ mice at 4 months. Data are mean ± SE; n ≥ 6; *p < 0.05 by t test.

(F) Average tumor area in small intestine and colon of *Apc*$^{Min/+}$/*IKKα*$^{WT/WT}$ and *Apc*$^{Min/+}$/*IKKα*$^{AA/AA}$ mice at 4 months. Data are mean ± SE; n ≥ 15 tumors of each genotype; *p < 0.05 by t test.

(G and H) Representative hematoxylin and eosin (H&E)-stained sections of colons from $Apc^{Min/+}/IKK\alpha^{WT/WT}$ (G) and $Apc^{Min/+}/IKK\alpha^{AA/AA}$ (H) mice at 4 months; scale bar = 1 mm. Arrowhead indicates adenoma.

(I and J) Hemoglobin (I) and hematocrit (J) levels of $Apc^{Min/+}/IKK\alpha^{WT/WT}$ and $Apc^{Min/+}/IKK\alpha^{AA/AA}$ mice at 4 months. Data are mean ± SE; $n \geq 5$ of each genotype; $^{**}p < 0.01$ and $^{*}p < 0.05$ by t test.

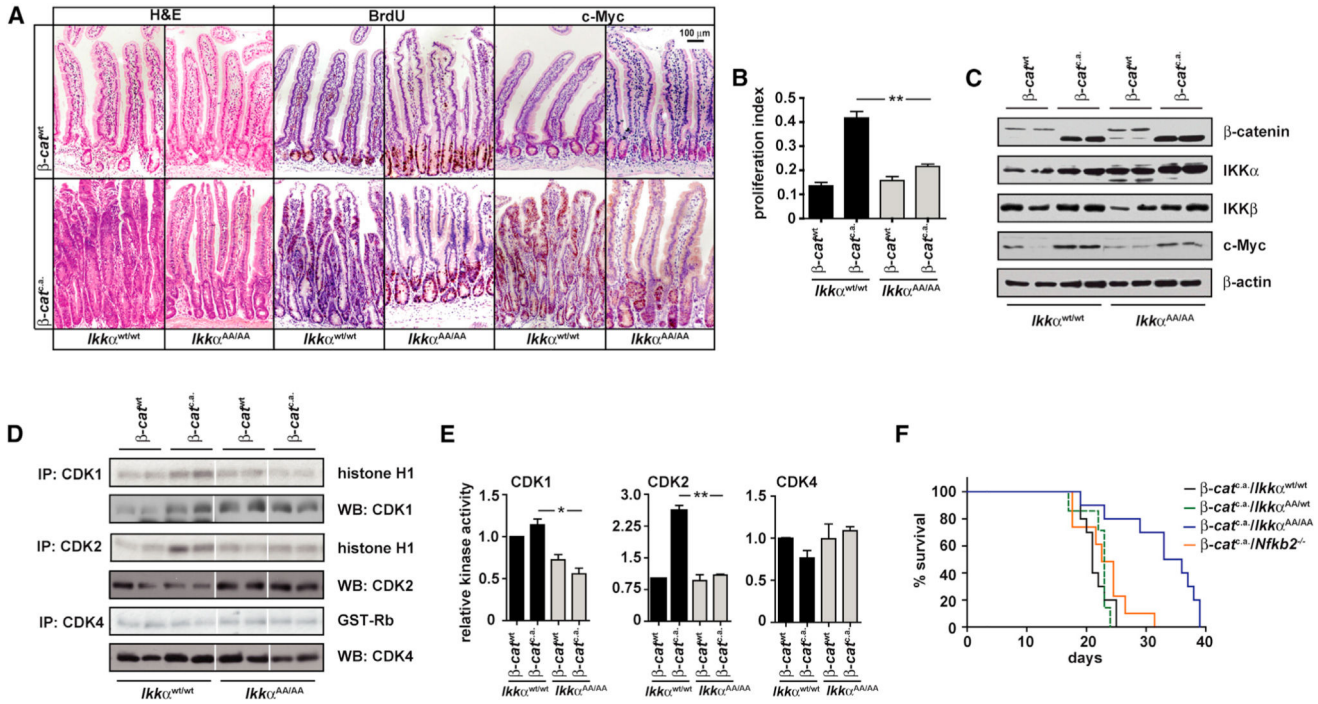

Figure 2. Reduced Proliferation in IKKα-Activation-Impaired Mice Is due to G1 Cell Cycle Arrest and Is Independent of Alternative NF-κB Activation

(A) H&E staining as well as immunohistochemical analysis of BrdU and c-Myc in small intestine of wild-type, *IKKα*$^{AA/AA}$, *β-cat*$^{c.a.}$, and *β-cat*$^{c.a.}$/*IKKα*$^{AA/AA}$ mice 15 days after the first tamoxifen application. The scale bar represents 100 μm.

(B) BrdU proliferation index of epithelial cells in unchallenged wild-type and *IKKα*$^{AA/AA}$ mice as well as *β-cat*$^{c.a.}$ and *β-cat*$^{c.a.}$/*IKKα*$^{AA/AA}$ mice 15 days after first tamoxifen administration. Data are mean ± SE; n = 3 for all genotypes; **p < 0.01 by t test.

(C) Immunoblot analysis of β-catenin, IKKα, IKKβ, and c-Myc in *β-cat*$^{c.a.}$/*IKKα*$^{WT/WT}$ and *β-cat*$^{c.a.}$/*IKKα*$^{AA/AA}$ mice IEC lysates at 0 or 15 days after first tamoxifen injection.

(D and E) Kinase assays (D), loading controls, and (E) loading-corrected relative kinase activities for endogenous CDK1, CDK2, and CDK4 in IEC from unchallenged wild-type and *IKKα*$^{AA/AA}$ mice as well as *β-cat*$^{c.a.}$ and *β-cat*$^{c.a.}$/*IKKα*$^{AA/AA}$ mice 15 days after first tamoxifen application. Data are mean ± SE; n = 2 for all genotypes; *p < 0.05 and **p < 0.01 by ANOVA followed by Bonferroni post hoc test for multiple data sets. GST, glutathione S-transferase; IP, immunopre-cipitation; WB, western blot.

(F) Kaplan-Meier survival graph for *β-cat*$^{c.a.}$/*IKKα*$^{WT/WT}$ (n = 11), *β-cat*$^{c.a.}$/*IKKα*$^{WT/AA}$ (n = 7), *β-cat*$^{c.a.}$/*IKKα*$^{AA/AA}$ (n = 10), and *β-cat*$^{c.a.}$/*Nfkb2*$^{-/-}$ (n = 8) mice; **p < 0.01 by log rank test.

See also Figure S1.

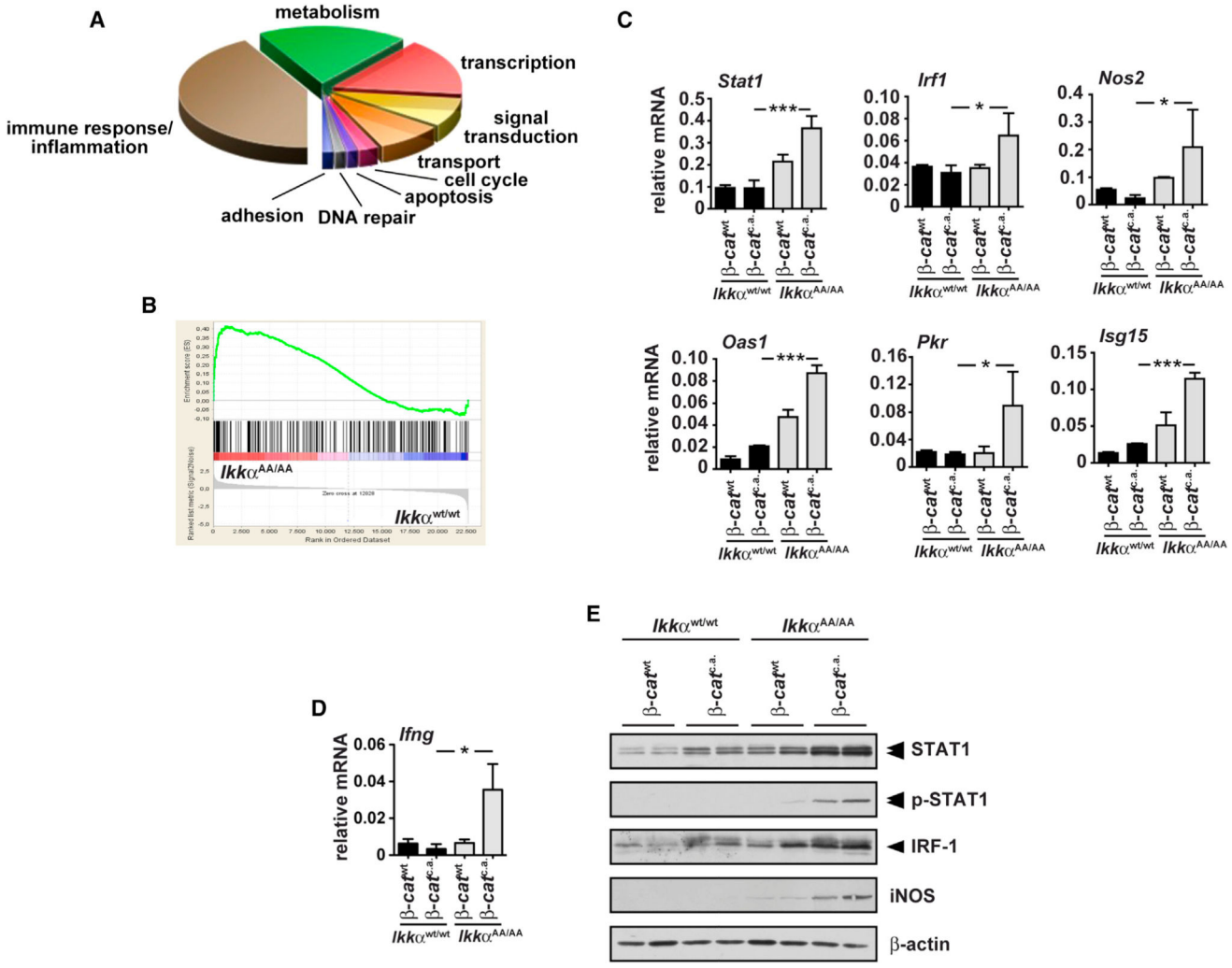

Figure 3. Generation of an IFNγ-Dominated Microenvironment in the Mucosa of *β-cat*$^{c.a.}$/*Ikkα*$^{AA/AA}$ Mice

(A) KEGG pathway analysis of the genes significantly upregulated in *β-cat*$^{c.a.}$/*Ikkα*$^{AA/AA}$ mice IECs 15 days after first tamoxifen administration.

(B) Gene set enrichment analysis (GSEA) comparing expression of all genes with a combined data set of interferon-regulated genes (Browne et al., 2001; Zhang et al., 2005; Bosco et al., 2010; Einav et al., 2005; Natsume et al., 2005; Reactome database; STKE database) in *β-cat*$^{c.a.}$/*Ikkα*$^{WT/WT}$ versus *β-cat*$^{c.a.}$/*Ikkα*$^{AA/AA}$ mice IECs 15 days after first tamoxifen injection; normalized enrichment score = 2.03; ***$p < 0.001$.

(C and D) Real-time PCR expression analysis of indicated genes in mucosa from wild-type, *Ikkα*$^{AA/AA}$, *β-cat*$^{c.a.}$, and *β-cat*$^{c.a.}$/*Ikkα*$^{AA/AA}$ mice 15 days after the first tamoxifen application. Data are mean ± SE; $n \geq 3$ for all genotypes. *$p < 0.05$; ***$p < 0.001$ by ANOVA followed by Bonferroni post hoc test for multiple data sets.

(E) Immunoblot analysis of IFNγ downstream targets p-STAT1, STAT1, IRF1, and iNOS in small-intestinal IEC from wild-type, *Ikkα*$^{AA/AA}$, *β-cat*$^{c.a.}$, and *β-cat*$^{c.a.}$/*Ikkα*$^{AA/AA}$ mice 15 days after the first tamoxifen application.

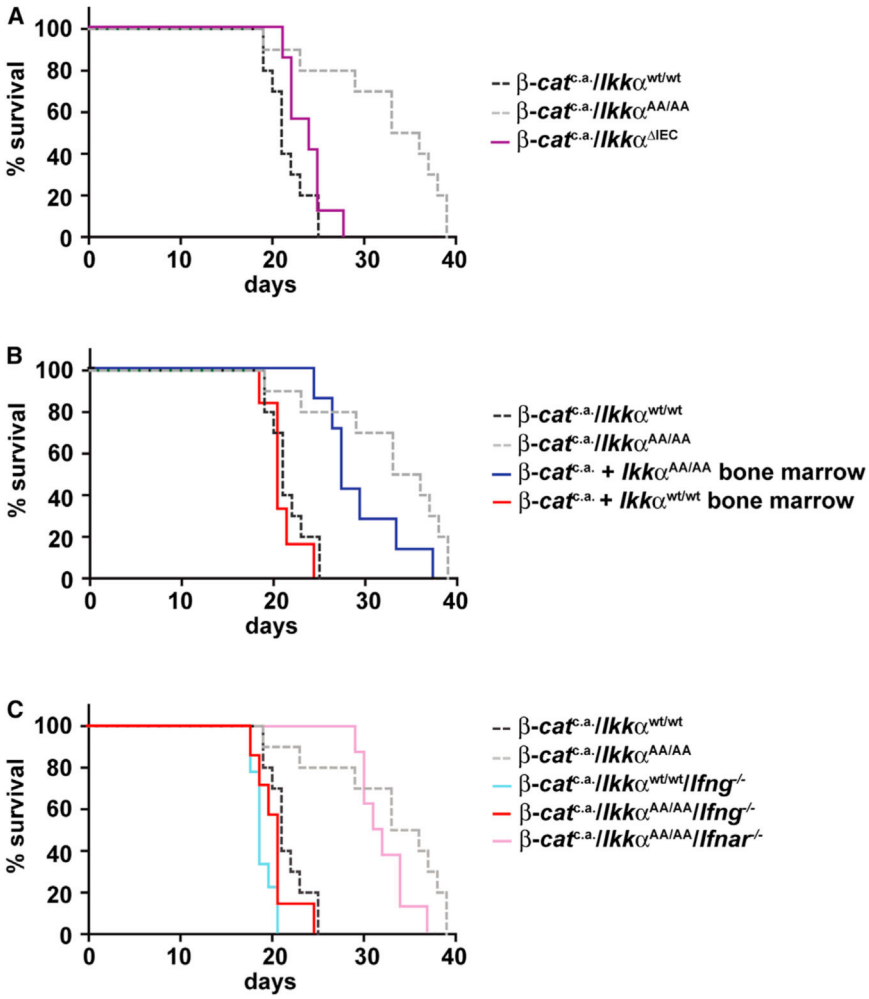

Figure 4. Improved Survival of *β-cat*$^{c.a.}$/*Ikkα*$^{AA/AA}$ Mice Depends on IFNγ

(A) Kaplan-Meier survival graph of *β-cat*$^{c.a.}$/*Ikkα*$^{\Delta IEC}$ mice (violet line). Survival of *β-cat*$^{c.a.}$/*Ikkα*$^{WT/WT}$ and *β-cat*$^{c.a.}$/*Ikkα*$^{AA/AA}$ mice shown as comparison (dashed gray lines; p = not significant [n.s.]).

(B) Kaplan-Meier survival graph of lethally irradiated *β-cat*$^{c.a.}$/*Ikkα*$^{WT/WT}$ mice transplanted with either *Ikkα*$^{WT/WT}$ (n = 6; red line) or *Ikkα*$^{AA/AA}$ (n = 7; blue line) bone marrow; ***p < 0.001 by log rank test.

(C) Kaplan-Meier survival graph of *β-cat*$^{c.a.}$/*Ikkα*$^{WT/WT}$/*Ifng*$^{-/-}$ (n = 9; light blue line), *β-cat*$^{c.a.}$/*Ikkα*$^{AA/AA}$/*Ifng*$^{-/-}$ (n = 5; red line; **p < 0.005), and *β-cat*$^{c.a.}$/*Ikkα*$^{AA/AA}$/ *Ifnar1*$^{-/-}$ mice (n = 8; pink line; p > 0.05) mice. Survival of *β-cat*$^{c.a.}$/*Ikkα*$^{WT/WT}$ and *β-cat*$^{c.a.}$/*Ikkα*$^{AA/AA}$ mice shown as comparison (dashed gray lines).

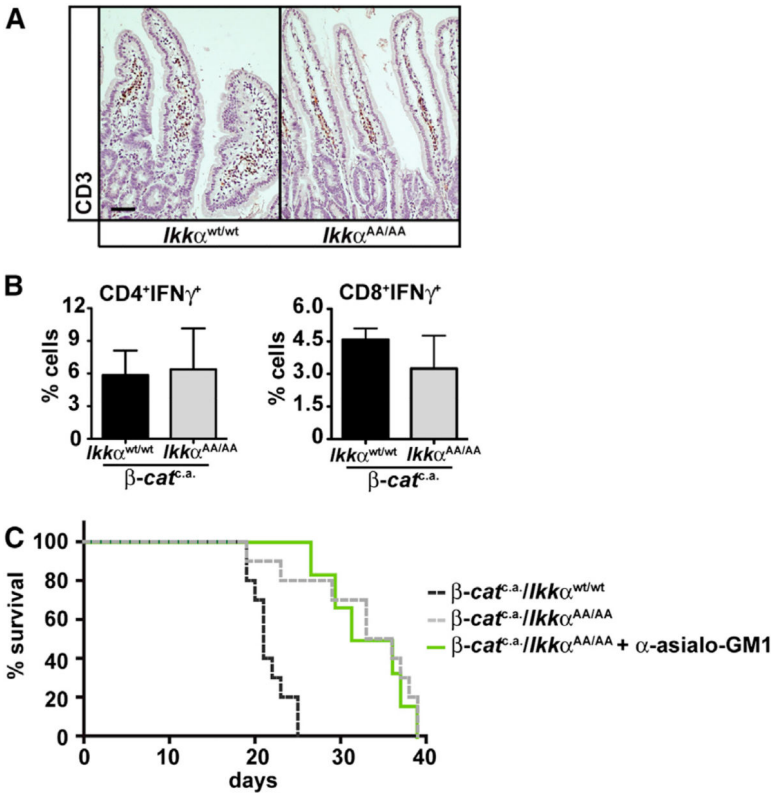

Figure 5. IKKα Mutant T Cells and NK Cells Do Not Contribute to Elevated IFNγ Expression in *β-cat*$^{c.a.}$ Mice

(A) Immunohistochemical analysis of CD3 in small intestine of *β-cat*$^{c.a.}$ and *β-cat*$^{c.a.}$/*Ikkα*$^{AA/AA}$ mice 15 days after the first tamoxifen application. The scale bar represents 100 μm.

(B) FACS analysis of $CD4^+IFN\gamma^+$ or $CD8^+IFN\gamma^+$ mucosa infiltrating lymphoid cells isolated from *β-cat*$^{c.a.}$/*Ikkα*$^{WT/WT}$ and *β-cat*$^{c.a.}$/*Ikkα*$^{AA/AA}$ mice small intestinal mucosa 15 days after first tamoxifen administration. T cells were restimulated using PMA (20 ng/ml) and ionomycin (1 μg/ml) for 6 hr in the presence of Brefeldin A. Data are mean ± SE; n = 2.

(C) Kaplan-Meier survival graph of *β-cat*$^{c.a.}$/*Ikkα*$^{AA/AA}$ mice injected with a-asialo-GM1 antibody (n = 6; green line). Survival of *β-cat*$^{c.a.}$/*Ikkα*$^{WT/WT}$ and *β-cat*$^{c.a.}$/*Ikkα*$^{AA/AA}$ mice shown as comparison (dashed gray lines; p = n.s.).

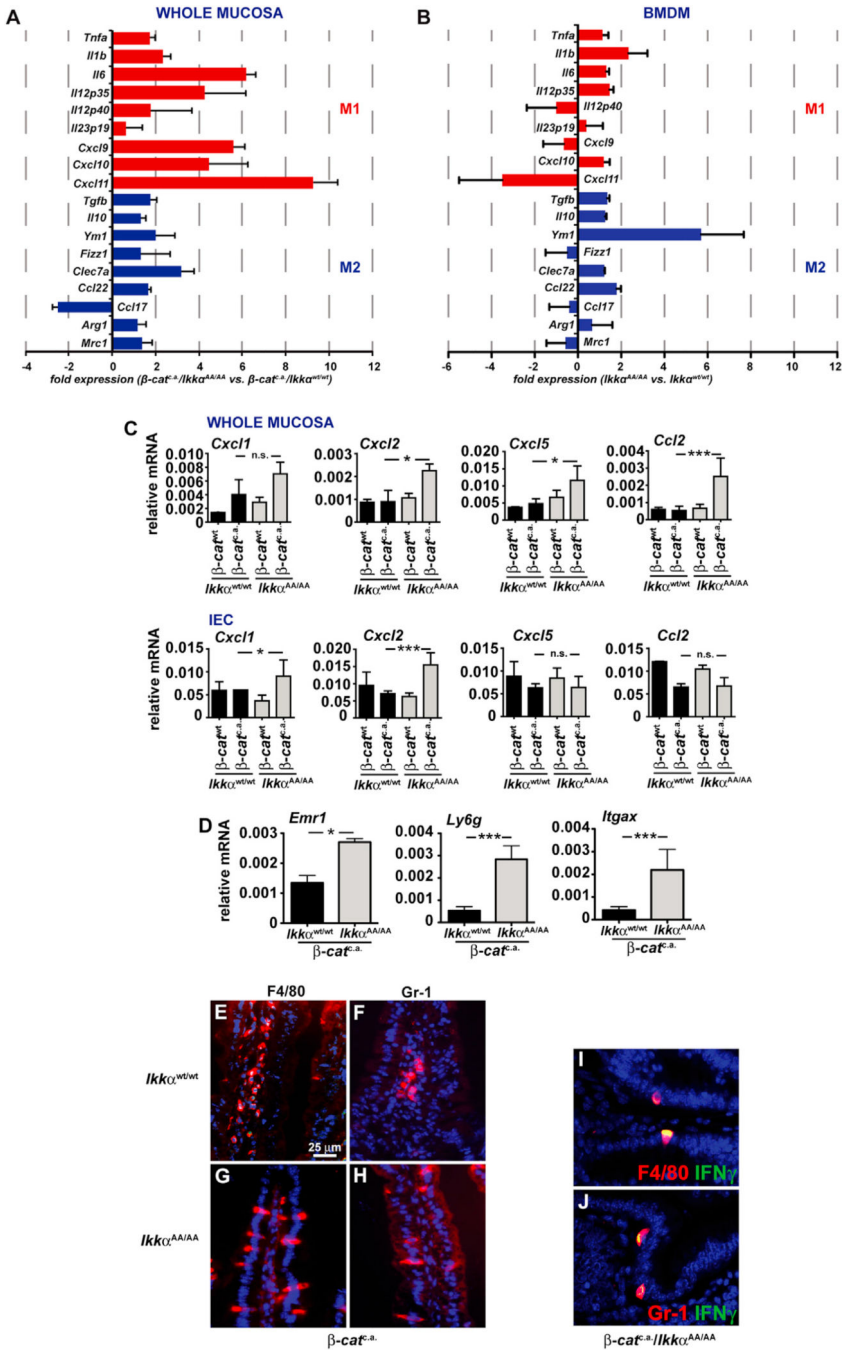

Figure 6. M1-like Polarized Myeloid Cells Are Source of IFNγ in β-*cat*$^{c.a.}$/*Ikkα*$^{AA/AA}$ Mice

(A) Real-time PCR expression analysis of M1 (red) and M2 (blue) macrophage markers in lamina propria samples from *β-cat*$^{c.a.}$/*Ikkα*$^{WT/WT}$ and *β-cat*$^{c.a.}$/*Ikkα*$^{AA/AA}$ mice 15 days after first tamoxifen administration. Data shown represent fold difference of Ct values from *β-cat*$^{c.a.}$/*Ikkα*$^{AA/AA}$ versus *β-cat*$^{c.a.}$/*Ikkα*$^{WT/WT}$ mice. Data are mean ± SE; n ≥ 3 for both genotypes.

(B) Real-time PCR expression analysis of M1 (red) and M2 (blue) macrophage markers in bone-marrow-derived macrophages (BMDM) from *Ikkα*$^{WT/WT}$ and *Ikkα*$^{AA/AA}$ mice that

have been stimulated with a mix of IFNγ (5 ng/ml) and lipopolysaccharide (100 ng/ml; M1 markers) or IL-4 (10 ng/ml; M2 markers) for 4 hr. Data shown represent fold difference of Ct values from *Ikkα*$^{AA/AA}$ versus *Ikkα*$^{WT/WT}$ mice. Data are mean ± SE; n = 3 for both genotypes.

(C) Real-time PCR expression analysis of chemokines *Cxcl1*, *Cxl2*, *Cxcl5*, and *Ccl2* in whole mucosa samples or IEC from unchallenged wild-type and *Ikkα*$^{AA/AA}$ mice as well as *β-cat*$^{c.a.}$ and *β-cat*$^{c.a.}$/*Ikkα*$^{AA/AA}$ mice 15 days after first tamoxifen application. Data are mean ± SE; n ≥ 3 for all genotypes. *p < 0.05, ***p < 0.001 by ANOVA followed by Bonferroni post hoc test for multiple data sets.

(D) RT-PCR expression analysis of myeloid cell markers *Emr1*, *Ly6g*, and *Itgax* in whole mucosa samples from unchallenged wild-type and *Ikkα*$^{AA/AA}$ mice as well as *β-cat*$^{c.a.}$ and *β-cat*$^{c.a.}$/*Ikkα*$^{AA/AA}$ mice 15 days after first tamoxifen application. Data are mean ± SE; n ≥ 3 for all genotypes. *p < 0.05; ***p < 0.001 by t test.

(E–H) Immunofluorescence staining of myeloid cell markers F4/80 (E and G) and Gr-1 (F and H) in small intestine of *β-cat*$^{c.a.}$/*Ikkα*$^{WT/WT}$ and *β-cat*$^{c.a.}$/*Ikkα*$^{AA/AA}$ mice 15 days after first tamoxifen application. The scale bar represents 25 μm.

(I and J) Coimmunofluorescence of F4/80 and IFNγ (I) as well as Gr-1 and IFNγ (J) in small intestine of *β-cat*$^{c.a.}$/*Ikkα*$^{AA/AA}$ mice 15 days after first tamoxifen application.

See also Figure S2.

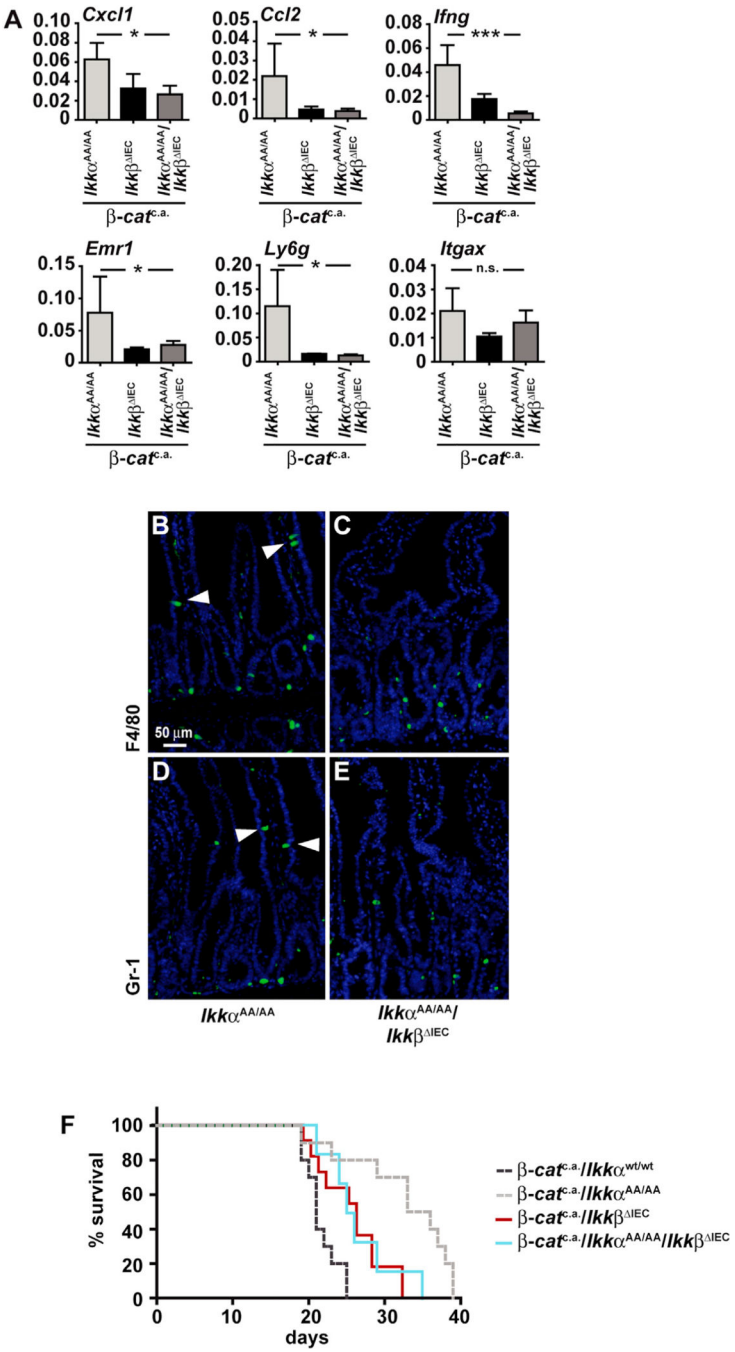

Figure 7. Enhanced Recruitment and Activation of Myeloid Cells in *β-cat*$^{c.a.}$/*Ikkα*$^{AA/AA}$ Mice Depend on IKKβ-Dependent NF-κB Activation in IEC

(A) Real-time PCR analysis of indicated genes in *β-cat*$^{c.a.}$/*Ikkα*$^{WT/WT}$, *β-cat*$^{c.a.}$/*Ikkα*$^{AA/AA}$, and *β-cat*$^{c.a.}$/*Ikkα*$^{AA/AA}$/*Ikkβ*$^{\Delta IEC}$ mice whole mucosa samples 15 days after first tamoxifen application. Data are mean ± SE; n ≥ 3 for all genotypes. *p < 0.05; ***p < 0.001 by ANOVA followed by Bonferroni post hoc test for multiple data sets.

(B–E) Immunofluorescent staining of F4/80 (B and C) and Gr-1 (D and E) in small intestine of *β-cat*$^{c.a.}$/*Ikkα*$^{AA/AA}$ and *β-cat*$^{c.a.}$/*Ikkα*$^{AA/AA}$/*Ikkβ*$^{\Delta IEC}$ mice 15 days after first tamoxifen administration. The scale bar represents 50 μm.

(F) Kaplan-Meier survival graph of $\beta\text{-}cat^{c.a.}/Ikk\beta^{\Delta IEC}$ (n = 11; red line) and $\beta\text{-}cat^{c.a.}/Ikk\alpha^{AA/AA}/Ikk\beta^{\Delta IEC}$ mice (n = 6; blue line). Survival of $\beta\text{-}cat^{c.a.}/Ikk\alpha^{WT/WT}$ and $\beta\text{-}cat^{c.a.}/Ikk\alpha^{AA/AA}$ mice shown as comparison (dashed gray lines).